ELSEVIER

Journal of Nuclear Materials 250 (1997) 36–52

journal of nuclear materials

In situ studies of ion irradiated zirconolite, pyrochlore and perovskite

Katherine L. Smith [a,*], Nestor J. Zaluzec [b], Gregory R. Lumpkin [a]

[a] *Materials Division, Australian Nuclear Science and Technology Organisation, P.M.B. 1, Menai, NSW 2234, Australia*
[b] *Materials Science Division, Argonne National Laboratory, 9700 South Cass Avenue, Argonne, IL, USA*

Received 20 December 1996; accepted 7 July 1997

Abstract

The relative radiation resistance of the structures of zirconolite, pyrochlore and perovksite were investigated by in situ transmission electron microscopy using 1.5 MeV Kr^+ ions in the HVEM-Tandem User Facility, at Argonne National Laboratory. A suite of six fabricated zirconolites, one fabricated pyrochlore and one natural perovskite was used. Damage accumulation essentially occurs in the same way in all three phases and is revealed by the following changes in SAD patterns: weakening of superlattice Bragg diffraction maxima, appearance of diffuse rings which increase in intensity with dose, disappearance of superlattice or other specific classes of maxima, and disappearance of remaining sublattice maxima leaving only diffuse rings. The average critical doses for amorphisation (D_c) for all the zirconolites (undoped, Nd-doped, U-doped and Th-doped) and the pyrochlore in this study varied by a factor of ~ 2 (from 3.5 to 6.1×10^{18} ions m^{-2}). No correlations were observed between D_c and the atomic weight of dopants in zirconolite or the mean atomic weight of the sample. The D_c value at room temperature of perovskite was found to be 1.8×10^{19} ions m^{-2}, 3–5 times the D_c values for zirconolite. This observation is in line with what one expects from the topologic and chemical complexity of the two phases and is compared with the results of previous authors. Preliminary assessment was made of EELS as a tool for monitoring radiation damage. © 1997 Elsevier Science B.V.

PACS: 61.80.−x; 61.80.Jh; 61.72.Ff; 81.05.Je

1. Introduction

Zirconolite (nominally $CaZrTi_2O_7$), pyrochlore ($^{VIII}A_2{}^{VI}B_2{}^{IV}X_6Y$) and perovskite (nominally $CaTiO_3$) are candidate phases for the immobilization, in dilute solid solution, of rare earth elements (REEs), fission products and actinides (ACTs) in various high level radioactive waste (HLW) forms [1]. Alpha decay of incorporated actinides causes self damage in HLW forms, and leads to a crystalline to amorphous transformation in zirconolite, pyrochlore and perovskite at doses of ~ 1 dpa. The effect of radiation damage on the structure of these phases (and consequently on their leachability) is important for predictive modelling of their behaviour in the repository environment and risk assessment. Of these three phases, zirconolite is likely to be the preferred host phase because it is more dissolution resistant than perovskite (e.g., [2]) and because studies of mineral analogues suggest that amorphous zirconolite is more resistant to aqueous alteration than amorphous pyrochlore (e.g., [3]).

Radiation damage effects in candidate HLW phases can be investigated by examining metamict and partly metamict mineral analogues (e.g., [4]) but such studies are limited by the availability of natural samples. Alternatively, as the work of previous authors has shown, long term radiation damage effects in candidate HLW phases can be simulated:

(i) by doping with high levels of short-lived radioactive transuranic isotopes (e.g., [5–7]),

(ii) by irradiating with fast neutrons (e.g., [8]) or

(iii) by irradiating with energetic ions (e.g., [9,10]) including 1.0 and 1.5 MeV Kr^+ ions [11,12].

* Corresponding author. Tel.: +61-2 9717 3448; fax: +61-2 9543 7179; e-mail: kls@ansto.gov.au.

PII S0022-3115(97)00237-7

Samples doped with high levels of short lived radioactive species or irradiated with neutrons are radioactive. Characterisation of radioactive samples is time consuming, as they must be handled according to rigorous safety regulations often using dedicated equipment.

In this study, long term radiation damage effects at room temperature in six fabricated zirconolites (of various compositions and structures), one fabricated pyrochlore and one natural perovskite were simulated by irradiating samples with 1.5 MeV Kr^+ ions using the HVEM-Tandem Facility at Argonne National Laboratory. Samples were monitored before, during and after irradiation using selected area electron diffraction (SAD) and were examined before and after irradiation using electron energy loss spectroscopy (EELS) and analytical transmission electron microscopy (AEM). The computer program TRIM (transport of ions in materials [13]), which calculates the transport of energetic ions into and through target materials, was used to calculate displacements/ion/nm as a function of depth in zirconolite irradiated with 1.5 MeV Kr^+ ions. These calculations are discussed in relation to the experimental results.

This work was undertaken in order to ascertain the effect of composition and structure on radiation damage in zirconolite and to compare the relative radiation resistance (i.e., the critical dose for amorphisation at room temperature) of zirconolite, pyrochlore and perovskite. In other studies, the radiation resistance of zirconolite and pyrochlore have always been found to be comparable (Section 5.3); whereas the relative radiation resistance of zirconolite and perovskite is less certain (Section 5.4). This study also allows preliminary assessment of EELS as a tool for monitoring radiation damage.

2. The crystal structures of zirconolite, pyrochlore and perovskite

Zirconolite (nominally $CaZrTi_2O_7$) and pyrochlore ($^{VIII}A_2{}^{VI}B_2{}^{IV}X_6Y$) are both anion deficient superstructures based on the fluorite structure (MX_2, where M is a cation and X is an anion) [14]. They can both be described as layer structures wherein every second layer is a hexagonal tungsten bronze (HTB) type layer predominantly composed of octahedrally coordinated cations. In zirconolite the layers are parallel to (001) while in pyrochlore they are parallel to (111).

Zirconolite occurs as various polytypes. Zirconolite-2M, zirconolite-3T and zirconolite-4M (nomenclature according to Bayliss et al. [15]) contain two, three and four HTB-type layers, respectively [14]. The calcium end-member ($CaZrTi_2O_7$) and samples containing low levels of rare earth elements (REEs) and/or actinides (ACTs) occur as the monoclinic structure, zirconolite-2M. Zirconolites doped with ~ 22 wt% Nd_2O_3 or ~ 14 wt% ThO_2 exhibit the trigonal structure, zirconolite-3T. Samples containing high levels (< 18 wt%) of REEs exhibit the monoclinic zirconolite-4M structure. When the solid solution limit of rare earth elements (REEs) or actinides (ACTs) in zirconolite is exceeded then pyrochlore is formed [16,17]. The major difference between zirconolite and pyrochlore, is that pyrochlore is expanded (by $\sim 4\%$) along the zirconolite c^* axis (the pyrochlore [111] axis) relative to zirconolite. In other words, pyrochlore can be thought of as an 'expanded zirconolite'.

Perovskite (nominally $CaTiO_3$) is composed of corner-linked TiO_6 octahedra with the calcium site located in the centre of a large cavity formed by eight TiO_6 octahedra [18]. Cations occupying the Ca site are twelvefold coordinated.

3. Experimental methods

3.1. Sample fabrication

Undoped, Nd-doped and Th-doped zirconolites were prepared by grinding up and pelletising appropriate mixtures of $CaCO_3$, TiO_2, ZrO_2 and Nd_2O_3; these pellets were then sintered in air at temperatures between 1300–1520°C. Compositional information and fabrication details are given in Table 1.

The U-doped zirconolite and U-doped pyrochlore were made by mixing Ti and Zr alkoxides with aqueous calcium and uranyl nitrate solutions and, in the case of zirconolite, Al nitrate solutions. These mixtures were stir-dried, calcined in 3.5% H_2/N_2 at ~ 700°C (to remove water, nitrates and organics), uniaxially hot-pressed in graphite dies at 1250°C and then fired in air at 1350°C to enhance phase development and minimise perovskite formation [19].

The perovskite is a natural sample from the Ural Mountains in Siberia, supplied to the authors by the Academy of Natural Sciences, Philadelphia (catalogue No. ANSP 24127).

3.2. TEM specimen preparation

Specimens for transmission electron microscopy (TEM) and in situ ion irradiation were prepared by crushing or ion beam thinning. Using the former method, samples were crushed under either acetone or ethanol using a small agate mortar and pestle, then holey carbon coated copper grids were carefully passed through the suspension to collect fine particles on the carbon film. Ion beam thinned (IBT) specimens were prepared by eroding 3 mm diameter dimpled discs with 4 kV Ar^+ ions incident at an angle of $\sim 20°$ to the surface of the specimen using a Gatan Duo Mill.

3.3. Elemental analyses

Elemental analyses of the zirconolite and pyrochlore specimens were performed after fabrication using a JEOL

Table 1
Compositions, fabrication details, dopant levels and critical amorphisation doses of samples in this study and in that of White et al. [11]

Full sample description, average composition	Fabrication details	Mean atomic number	Critical dose for amorphisation (10^{18} ions m^{-2})	Number of grains monitored
Data relating to samples irradiated with 1.5 MeV Kr^+ ions at room temperature in this study				
Undoped zirconolite-2M $(Ca_{0.96}Zr_{0.01})_{0.97}Zr_{1.00}(Ti_{1.95}Zr_{0.05})_{2.00}O_{7.00}$	sintered at 1300°C for 48 h	14.6	5.5 ± 1.3	6
Nd-doped zirconolite-2M $(Ca_{0.81}Nd_{0.17})_{0.98}Zr_{0.97}(Ti_{1.89}Zr_{0.11})_{2.00}O_{7.00}$	sintered at 1400°C for 8 h	15.2	5.3 ± 0.7	3
Nd-doped zirconolite-3T $(Ca_{0.77}Nd_{0.19})_{0.96}Zr_{0.97}(Ti_{1.89}Zr_{0.11})_{2.00}O_{7.00}$	sintered at 1400°C for 4 h	15.3	3.9 ± 0.5	5
Nd-doped zirconolite-4M (TEM specimens prepared by crushing) $(Ca_{0.71}Nd_{0.27})_{0.98}(Zr_{0.79}Nd_{0.21})_{1.00}(Ti_{1.96}Zr_{0.04})_{2.00}O_{7.00}$	sintered at 1380°C for 4 h	16.0	3.7 ± 0.3	3
Nd-doped zirconolite-4M (TEM specimens prepared by ion beam thinning) $(Ca_{0.71}Nd_{0.27})_{0.98}(Zr_{0.79}Nd_{0.21})_{1.00}(Ti_{1.96}Zr_{0.04})_{2.00}O_{7.00}$	sintered at 1380°C for 4 h	16.0	3.5 ± 0.3	3
Nd-doped zirconolite-4M $(Ca_{0.71}Nd_{0.27})_{0.98}(Zr_{0.79}Nd_{0.21})_{1.00}(Ti_{1.96}Zr_{0.04})_{2.00}O_{7.00}$	sintered at 1380°C for 4 h	16.0	3.6 ± 0.2 [a]	6
U-doped zirconolite-2M $(Ca_{0.88}U_{0.08})_{0.96}(Zr_{0.99}U_{0.01})_{1.00}(Ti_{1.76}Al_{0.23}Zn_{0.01})_{2.00}O_{7.00}$	HUPed [b] in N_2 at 1250°C then fired in air at 1350°C	14.9	3.8 ± 0.5	4
U-doped pyrochlore $(Ca_{0.87}U_{0.62})_{1.49}(Ti_{1.76}Zr_{0.24})_{2.00}O_{6.72}$	HUPed [b] in N_2 at 1250°C then fired in air at 1350°C	17.3	4.1 ± 0.3	3
Th-doped zirconolite-3T $(Ca_{0.82}Th_{0.10})_{0.92}(Zr_{0.89}Th_{0.11})_{1.00}(Ti_{1.52}Zr_{0.48})_{2.00}O_{7.00}$	sintered at 1510°C for 10 d then sintered at 1520°C for 10 d	16.5	6.1 ± 0.3	3
Perovskite $Ca_{1.02}(Ti_{0.97}Fe_{0.01})_{0.98}O_{3.00}$	natural sample from the Ural Mtns, Siberia, ANSP 24127	13.2	18 ± 0.9	3
Data relating to samples irradiated with 1.0 MeV Kr^+ ions at room temperature by White et al. [11].				
Undoped zirconolite $CaZrTi_2O_7$	HUPed [b] in N_2 at 1100°C and ~ 20 MPa for 1 h	14.5	10.0	1
Gd-doped zirconolite $Ca_{0.75}Gd_{0.50}Zr_{0.75}Ti_2O_7$	HUPed [b] in N_2 at 1100°C and ~ 20 MPa for 1 h	16.1	6.8	1
U-doped zirconolite $Ca_{0.75}U_{0.5}Zr_{0.75}Ti_2O_7$	HUPed [b] in N_2 at 1100°C and ~ 20 MPa for 1 h	17.4	[c]	1

[a] Average of all Nd-doped zirconolite-4M data for crushed and ion beam thinned specimens.
[b] Hot isostatically pressed in a graphite die.
[c] Rendered amorphous during argon ion thinning in preparation for and prior to TEM investigation.

2000FX analytical transmission electron microscope (AEM) operated at 200 kV and fitted with a hybrid energy dispersive spectrometer (EDS) comprised of a high take-off angle (72°) Tracor Northern detector (with a 7.6 μm beryllium window) and a Link Isis analyser [20].

The zirconolite chemical formulae given in Table 1 were calculated on the basis of seven oxygen atoms. Cations of smaller radii (e.g., Ti, Zr, Al) were assigned to first fill the smaller cation sites (the Ti and Zr sites) and then the remaining cations were assigned to the Ca site. Based on their ionic size, it was assumed that the dopant atoms, Nd, U and Th, would only partition into the Ca and Zr sites.

X-ray diffraction established that the U-doped pyrochlore had the pyrochlore structure (cell edge 1.015 nm). The pyrochlore chemical formula given in Table 1 was calculated by assuming that there were two B-site cations per formula unit filled by Ti and Zr and that Ca and U occupied the A-site. Oxygen content was calculated by assuming that Ti, Zr, U and Ca had valences of 4^+, 4^+, 4^+ and 2^+ respectively.

The perovskite sample for irradiation was selected on the basis of scanning electron microscope (SEM) and EDS data, collected using a JEOL 6400 SEM fitted with a Tracor Northern EDS, and which showed that the sample is homogeneous with a composition close to that of the perovskite endmember, $CaTiO_3$. The composition given in Table 1 was calculated on the basis of three oxygen atoms, from SEM/EDS data.

3.4. In situ ion irradiation

In situ irradiations of TEM specimens were performed using a 1.2 MeV modified Kratos/AEI EM7 electron microscope (operated at 300 kV) interfaced with two National Electrostatics Corporation ion accelerators in the HVEM-Tandem Facility at Argonne National Laboratory. In this facility, the electron beam travels vertically down through the specimen and the irradiating ion beam is incident on the specimen at 30° to the vertical.

Grains chosen for irradiation were always electron transparent under bright field imaging at 300 kV. On the basis of convergent beam diffraction analysis of representative areas, we estimate that the thickness of the areas of grains from which we took SAD patterns was 60 ± 10 nm.

In general, zirconolite grains selected for observation during irradiation were aligned such that their [110] axes were parallel to the electron beam. The [110] zone axis was chosen because selected area electron diffraction (SAD) patterns of this zone contain bot:

(i) 'fluorite sub-lattice' Bragg diffraction maxima (the family of maxima derived from the zirconolite-2M (004), $(2\bar{2}1)$ and $(2\bar{2}\bar{3})$ maxima, and

(ii) 'zirconolite superlattice' Bragg diffraction maxima (those maxima derived from the (100) and $(1\bar{1}0)$ zirconolite maxima, other than the fluorite sublattice maxima; and maxima where (hkl): $h = -k = 2n + 1$).

When no grains of this orientation were available, other low-order zones were used. The [110] axis of zirconolite corresponds to the $[0\bar{1}1]$ axis of pyrochlore. So that we could directly compare zirconolite and pyrochlore results, we monitored pyrochlore grains whose $[0\bar{1}1]$ axes could be aligned parallel to the electron beam. The perovskite grains selected for observation during irradiation were aligned with a low-order zone parallel to the electron beam.

Three or more grains from one or more TEM specimens of each sample (i.e., composition or phase) were irradiated using the following procedure.

(i) Selected area diffraction (SAD) patterns and bright field images of a grain were recorded.

(ii) The electron beam was then turned off and the grain was irradiated with 1.5 MeV Kr^+ ions at a flux of $\sim 3.4 \times 10^{14}$ ions m^{-2} s^{-1} in increments of 1.7, 0.85 or 0.43×10^{18} ions m^{-2}. Weber et al. [21] showed that damage produced in non-actinide-bearing zircon by 1.5 MeV Kr^+ ions (at dose rates similar to that in this study) is comparable to alpha decay damage in U,Th-bearing natural zircons. Furthermore, the D_c of the ion irradiated zircon was comparable to that of the actinide-bearing zircons, despite that fact that the damage rate was $\sim 10^{13}$ times faster.

(iii) The Kr ion beam was then switched off, the electron beam was turned back on and the SAD pattern of the grain was re-recorded. If necessary, grains were re-aligned prior to re-recording their SAD patterns. Movement of grains necessitating realignment most probably results from buckling of the carbon film due to ion-induced breakdown of formvar left over from the manufacture of the film. Alternatively it could result from poor (thermal and/or electrical) connection of the grain to the holey carbon film and/or poor connection of the film to the copper support grid. These latter possibilities are discussed in more detail in Section 4.1.4.

This procedure was repeated until all Bragg diffraction maxima had disappeared and only diffuse rings remained in the SAD pattern. The dose at which this occurred was taken to be the critical dose for amorphisation, D_c.

All irradiation experiments were conducted nominally at room temperature. In similar experiments on ion beam thinned zirconolite samples, Ewing and Wang [12] monitored the specimen temperature with a thermocouple during 1.5 MeV Kr^+ ion irradiation and found that it did not exceed 55°C. Consequently, it can be assumed that, when there is good thermal connection between the grain and the holey carbon film and between the film and the support grid, then the temperature of the grains monitored in this study is ≤ 55°C.

3.5. TRIM based calculations

The program TRIM (transport of ions in materials [13]) Version 95.06 was used in full cascade mode (wherein all

interactions of the primary ion and all the recoil cascades are calculated) to calculate energy deposition due to nuclear (displacement and vacancies) and electronic (ionisation and phonons) processes as a function of depth in undoped zirconolite caused by 1.5 MeV Kr^+ ions (experimental conditions in this study) and 1.0 MeV Kr^+ ions (White et al.'s [11] experimental conditions). The density of zirconolite was taken to be 4.47×10^3 kg m^{-3}. This is the average density of the two undoped zirconolites (with compositions of $Ca_{0.993}Zr_{1.304}Ti_{1.700}O_7$ and $Ca_{0.961}Zr_{0.850}Ti_{2.169}O_7$) investigated by Gatehouse et al. [22]. The lattice binding energy (E_b) was assumed to be 2 eV. The average displacement energy (E_d) of atoms in zirconolite has not yet been determined. Ewing and coworkers (e.g., [12,10]) consistently use an E_d value of 15 eV for all ceramics; whereas Pells [23] listed average E_d values for ceramic insulators ranging from 45 to 56 eV. Calculations were therefore performed for E_d values of 15 and 50 eV. The displacements/ion/nm were calculated by adding the number of replacement collisions/ion/nm to the total number of vacancies/ion/nm. The displacements per atom (dpa) in undoped zirconolite irradiated with 1.5 MeV Kr^+ ions and 1.0 MeV Kr^+ ions at D_c were calculated based on: TRIM derived data; D_c values measured in this and White et al.'s [11] study; and the density of zirconolite.

TRIM calculations show that when a 60 nm thick zirconolite sample is irradiated with 1.5 MeV Kr^+ ions, the amount energy transferred to the sample which results in ionisation is up to 20 times that which results in atomic displacement. However, to our knowledge, zirconolite amorphisation has never been linked to electronic processes. Furthermore crystalline zirconolite does not become amorphous under the electron beam in an intermediate voltage (200–300 keV) TEM as do many ionisation-susceptible materials (e.g., quartz, hollandite). Consequently, in this study we only consider nuclear processes.

3.6. EELS

Electron energy loss (EEL) spectra were collected using a Philips 420 TEM (operated at 120 kV) that was fitted with a Gatan Model 607 serial EEL spectrometer (SEELS) with custom signal processing electronics and software. Spectra reported herein were recorded at resolutions of ~ 1.0 eV and at a dispersion of about ~ 0.25 eV/channel.

Four samples consisting of powdered material suspended on holey carbon grids were examined: undoped zirconolite-2M (Table 1), undoped zirconolite-2M which had been irradiated (as described above) until all the grains on the specimen grid were amorphous, reagent grade Ti_2O_3 (supplied by Merck, Darmstadt) and 99.9% pure TiO_2 (supplied by Cerac/Pure certified chemicals, Melbourne).

4. Results

4.1. In situ ion irradiation

4.1.1. Loss of order with dose in zirconolite

In general agreement with the work of White et al. [11], Ewing and Wang [12], Ewing and Headley [24] and Sinclair and Ringwood [25] increasing dose first caused the loss of zirconolite superlattice ordering and then the fluorite sublattice ordering. Loss of order with increasing dose is evidenced by the following changes which are exemplified in Fig. 1.

(i) Diminution of intensity of zirconolite superlattice (Bragg diffraction) maxima relative to the fluorite sublattice maxima (Fig. 1b).

(ii) The appearance of diffuse rings indicating spacings of ~ 0.29 and ~ 0.20 nm (Fig. 1d).

(iii) The disappearance of the zirconolite superlattice maxima (apart from the fluorite sublattice maxima) derived from the zirconolite (001) and $(2\bar{2}0)$ maxima (Fig. 1d).

(iv) The disappearance of layer lines where (hkl): $h = -k = 2n + 1$ (Fig. 1d).

(v) The disappearance of all remaining (fluorite sub-cell) maxima leaving only diffuse rings whose diameters are representative of the distance between first (M–O) and second (M–M) nearest neighbours (Fig. 1f).

Changes (i) and (v) are always the first and last stages respectively of the transition from the crystalline to the amorphous state. As mentioned above, the dose at which change (v) occurred was taken to be the critical dose for amorphisation (D_c). The D_c values of at least three samples of each composition and/or structure were averaged to give the values quoted in Table 1. The average D_c values at which all the zirconolites in this study became fully amorphous ranged from 3.5 to 6.1×10^{18} ions m^{-2}, that is they varied by a factor of ~ 2. The order of changes (ii) through (iv) was variable, dependent upon the specimen being studied.

The Bragg diffracted maxima in SAD patterns which persist to the highest doses are firstly those resulting from the fluorite sublattice and secondly the four (110)-type maxima which lie on the innermost of the two diffuse rings representative of amorphous zirconolite. These four maxima are the strongest (kinematic) maxima in unirradiated zirconolite.

4.1.2. Loss of order with dose in pyrochlore

The changes with dose observed in pyrochlore viewed down $[0\bar{1}1]$ are qualitatively similar to those seen in zirconolite viewed down [110]. With increasing dose, loss of order is evidenced by the following changes (exemplified in Fig. 2).

(i) The intensities of the 'fluorite sublattice' Bragg diffraction maxima increased relative to the 'pyrochlore

superlattice' maxima and diffuse rings appeared indicating spacings of ~0.29 and ~0.20 nm.

(ii) The following maxima disappeared: (hkk) where $h = 4n$ and $k = 4m + 2$, and (hkk) where $h = 4n + 2$ and $k = 4m$ (Fig. 2c).

(iii) Then the following maxima disappeared: (hkk) where $h = 2n + 1$ (Fig. 2c).

(iv) All remaining Bragg diffraction maxima disappeared, leaving only the diffuse rings (Fig. 2d).

The D_c values of three samples were averaged to give the value quoted in Table 1.

As was observed for zirconolite, the Bragg diffraction maxima in SAD patterns which persist to the highest doses are firstly those resulting from the fluorite sublattice and secondly the four (222) maxima which lie on the innermost of the two diffuse rings representative of amorphous pyrochlore. As was observed in zirconolite, the four maxima which persist to the highest doses are the strongest (kinematic) maxima in unirradiated pyrochlore.

4.1.3. Loss of order with dose in perovskite

The changes with dose observed in SAD patterns of perovskite are qualitatively similar to those seen in SAD patterns of zirconolite and pyrochlore: with increasing dose, diffuse rings representative of amorphous perovskite appear while concurrently some, then all classes of Bragg diffraction maxima disappear.

When a perovskite grain was viewed down [$\bar{1}$01], the following changes were observed with increasing dose (Fig. 3).

(i) The relative intensities of maxima in the SAD pattern changed (Fig. 3b).

(ii) The following maxima disappeared: ($0k0$), where $k = 2n + 1$ and $k = 4n + 2$, ($h0l$), $h = l = 2n + 1$, (hkl), where $k = 2n + 1$; or $h = l = 2n$ and $k = 4m + 2$; or $h = l = 2n + 1$ and $k = 4m$ (Fig. 3c).

(iii) Diffuse rings appeared indicating lattice spacings of ~0.29 and ~0.20 nm (Fig. 3c).

(iv) All remaining Bragg maxima disappeared leaving only the diffuse rings (Fig. 3d).

When a different perovskite grain was viewed down [010] the following sequential changes were observed with increasing dose (Fig. 4).

(i) The relative intensities of maxima in the SAD pattern changed (Fig. 4b).

(ii) Diffuse rings appeared indicating lattice spacings of ~0.29 and ~0.20 nm (Fig. 4d).

(iii) The following maxima disappeared: ($h00$), $h = 2n + 1$, ($00l$), $l = 2n + 1$, (hkl), $h + l = 2n + 1$ (Fig. 4d).

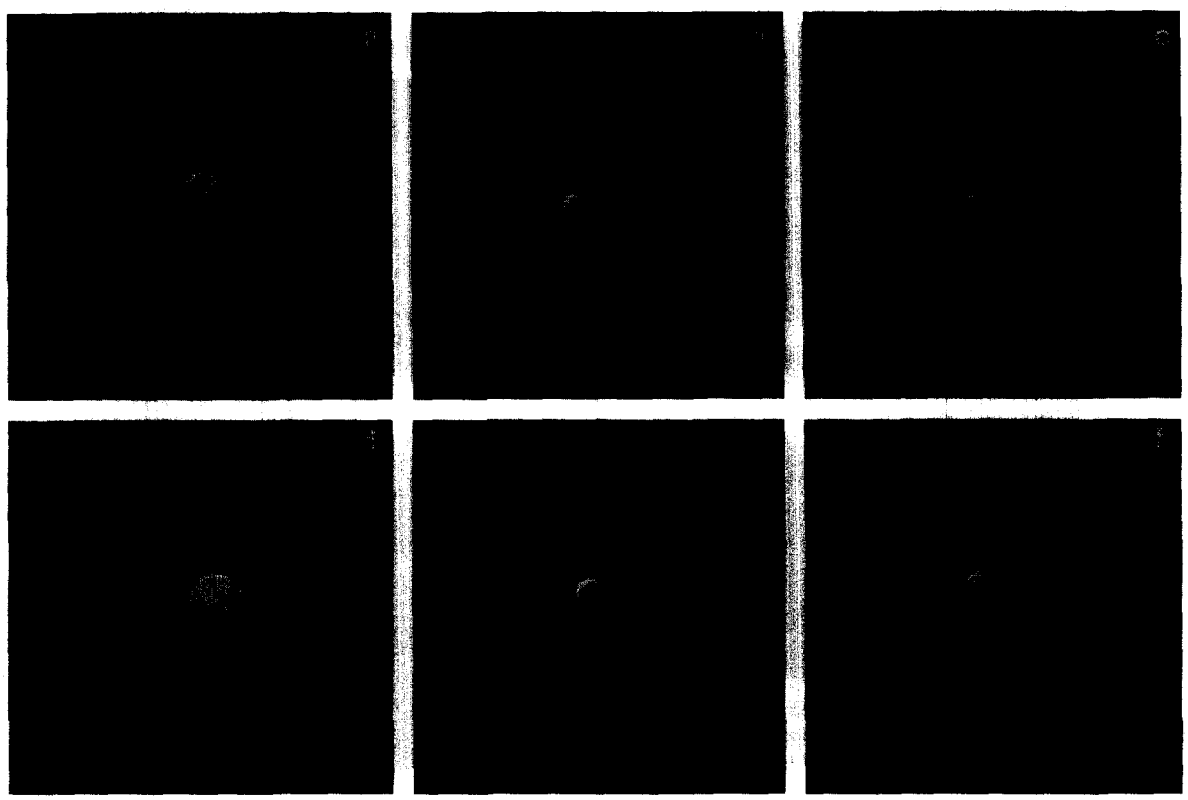

Fig. 1. SADs of a zirconolite-2M grain viewed down [110] showing the effect of increasing dose. (a) Before irradiation. (b) 0.85×10^{18} ions m^{-2}. (c) 2.6×10^{18} ions m^{-2}. The layer lines where (hkl): $h = -k = 2n + 1$ are faintly visible in the negative of this SAD. (d) 3.0×10^{18} ions m^{-2}. Faint diffuse rings are visible in the negative of this SAD. (e) 3.5×10^{18} ions m^{-2}. (f) 4.7×10^{18} ions m^{-2}.

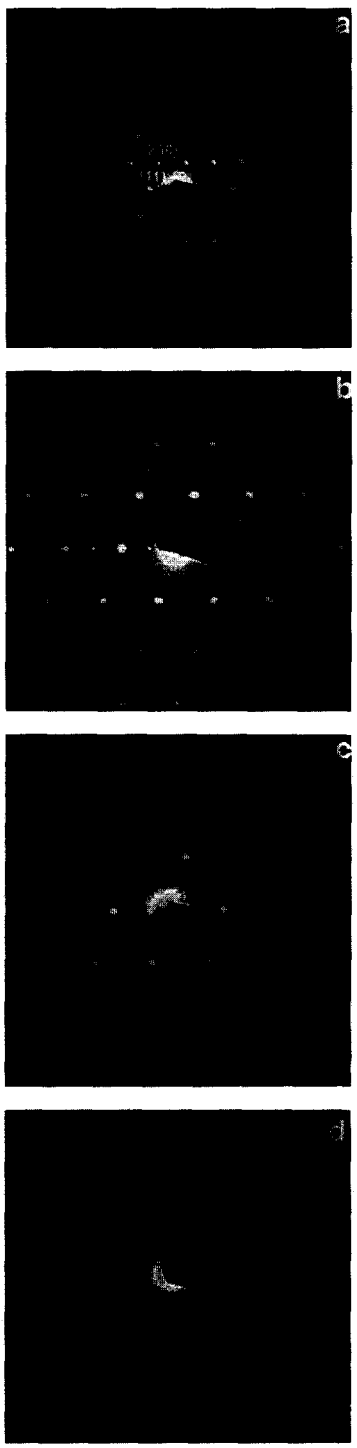

Fig. 2. SADs of a pyrochlore grain viewed down $[0\bar{1}1]$ showing the effect of increasing dose. (a) Before irradiation. (b) 1.7×10^{18} ions m^{-2}. (c) 2.6×10^{18} ions m^{-2}. (d) 4.3×10^{18} ions m^{-2}.

(iv) All remaining Bragg maxima disappeared leaving only the diffuse rings (Fig. 4e).

The D_c values of the samples shown in Figs. 3 and 4 were averaged to give the value quoted in Table 1. The doses at which (i) the relative intensities of SAD Bragg diffraction maxima first varied, (ii) diffuse rings first ap-

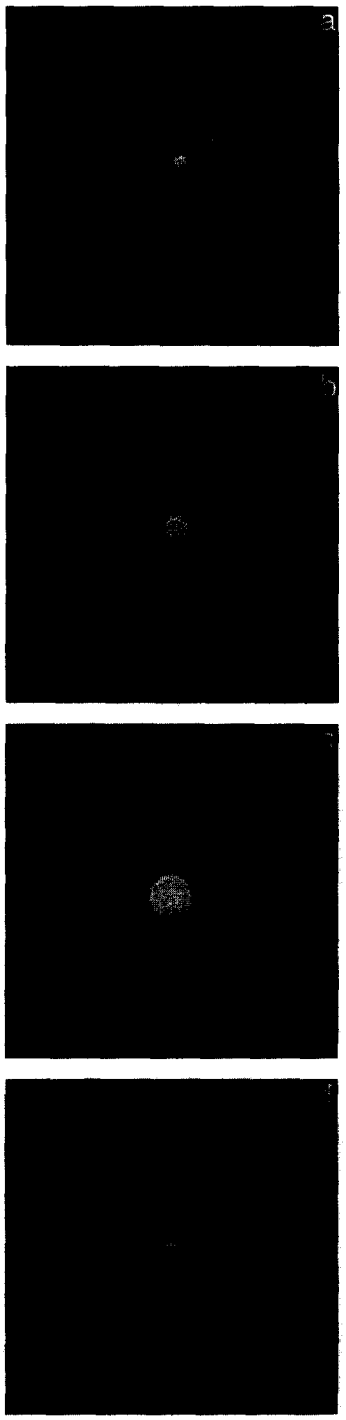

Fig. 3. SADs of a perovskite grain viewed down $[\bar{1}01]$ showing the effect of increasing dose. (a) Before irradiation. (b) 12.8×10^{18} ions m^{-2}. (c) 14.5×10^{18} ions m^{-2}. Faint diffuse rings are visible in the negative of this SAD. (d) 18.7×10^{18} ions m^{-2}.

peared and (iii) some (but not all) maxima disappeared, varied greatly.

The differences between Fig. 3a and b and between Fig. 4a and c are consistent with a change from orthorhombic to cubic symmetry. Such a symmetry change could be result from small shifts in the positions of the oxygen atoms similar to those postulated by Wittels and Sherrill [26].

As was observed for zirconolite and pyrochlore, the Bragg diffraction maxima which persisted to the highest doses are those on the innermost of the two diffuse rings representative of amorphous perovskite. Once again these were the strongest kinematic maxima in SAD patterns of undamaged perovskite. The diameters of the diffuse rings representative of amorphous perovskite are the same as those of amorphous zirconolite and pyrochlore.

4.1.4. Outliers

Approximately 15% of the monitored grains retained a degree of crystallinity after they had received much higher doses than that required to make other grains of the same sample become fully amorphous. We will refer to such grains as outliers. For example, one of the U-doped zirconolite-2M grains retained some crystallinity after a dose of 16.8×10^{18} ions m^{-2}; whereas three other grains were fully amorphous after doses of $\leq 4.3 \times 10^{18}$ ions m^{-2}.

Wang and co-workers have also observed outliers (Wang, personal communication, 1995). They attribute the

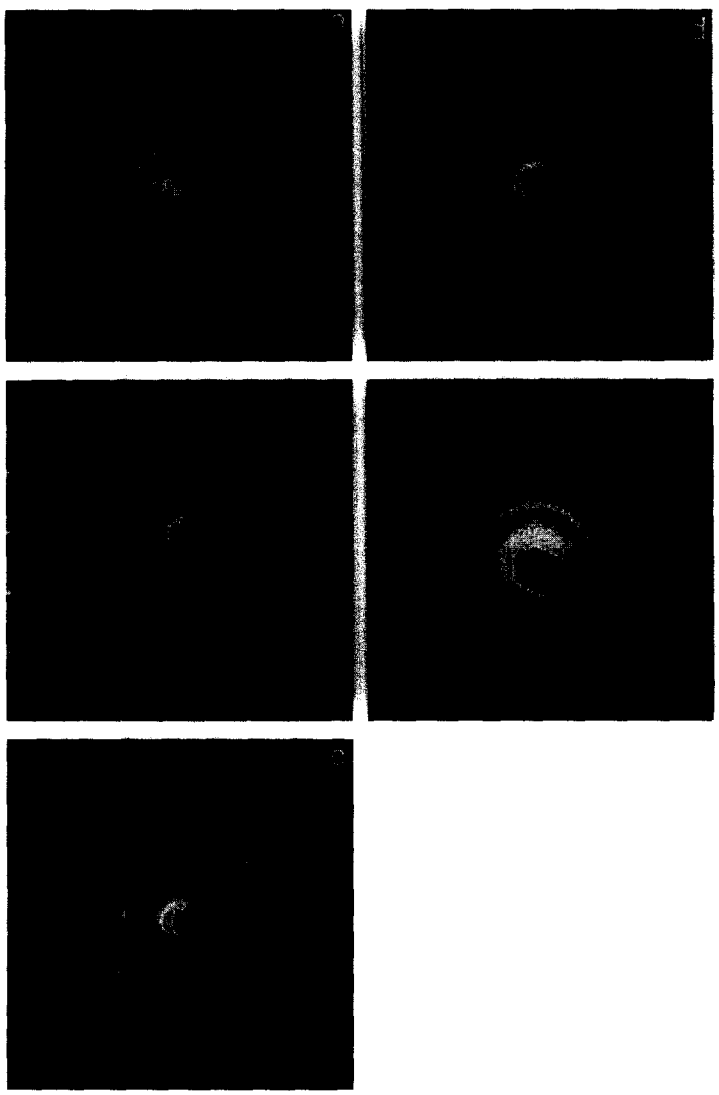

Fig. 4. SADs of a perovskite grain viewed down [010] showing the effect of increasing dose. (a) Before irradiation. (b) 3.4×10^{18} ions m^{-2}. (c) 6.8×10^{18} ions m^{-2}. (d) 10.0×10^{18} ions m^{-2}. (e) 17.0×10^{18} ions m^{-2}.

apparent radiation resistance of outliers to either electron beam annealing of specimens during ion irradiation (as documented by Koike et al. [27]) or elevated temperatures caused by poor thermal connection between the outlier and the holey carbon film and/or poor connection of the film to the copper support grid (which promotes annealing of damage [21,11]). Electron beam annealing during Kr^+ ion irradiation as reported by Koike et al. for intermetallic compounds may or may not apply to oxide ceramics but is not a consideration in this study, as the electron beam was always turned off whilst the samples were being irradiated with Kr^+ ions. Elevated temperatures in poorly attached grains can result from either Kr^+ ion irradiation or electron irradiation. However if the latter is the case in this study, annealing must occur so rapidly after the electron beam is turned back on that it is unobservable.

An alternative explanation of the apparent radiation resistance of outliers involves 'channeling' effects (e.g., [28]). Charged particles (e.g., 1.5 MeV Kr^+ ions) can channel (travel) through crystalline materials at certain orientations causing minimal damage. However this seems unlikely, as it appears to be difficult to induce electron channelling in zirconolite. Specifically, Turner et al. [29] used zone axis ALCHEMI (atom location by electron channelling enhanced microanalysis) to determine the location of minor elemental species on the different sites in the zirconolite unit cell. However, the zirconolite data they reported were collected in the vicinity of only one high-index unidentified zone axis, after they found that channelling effects were not observed in the vicinity of any low index zones (T.J. White, personal communication, 1994).

The apparent radiation resistance of the outliers in this study is unlikely to be due to shielding by parts of the specimen holder, microscope or accelerator assembly. Great care was taken to choose grains for SAD monitoring which lay close to the centre of the TEM samples and, in the case of samples suspended on holey-carbon-coated copper grids, in the centre of grid squares. Furthermore, it was found that the grains adjacent to outliers gave results consistent with the majority of grains of that sample.

The apparent radiation resistance of outliers in this study is also unlikely to be due to compositional variation, as the nominal compositions of the samples in this study were homogeneous.

In conclusion, the apparent radiation resistance of the outliers in this study is likely to be due to poor thermal connection between the individual grain and the holey carbon film. Consequently, in agreement with the practice of Wang and co-workers, we have not used the results from outliers to calculate average doses.

4.1.5. Comments on the D_c values measured in this study

The quoted errors in Table 1 are those values which need to be added or subtracted to the average dose to cover the entire range of experimental values of that phase, composition or structure. The data in Table 1 show that there is no correlation between D_c and the atomic weight of the dopant or between D_c and the mean atomic number of the sample (which is an indicator of the level of dopant substitution). This result was expected because previous studies of the amorphisation of complex silicates (Eby et al. [30], Wang et al. [31]) showed that density and atomic mass are not controlling properties for D_c. The D_c ranges of Nd-doped zirconolite-2M and Nd-doped zirconolite-3T do not overlap which might suggest a correlation between D_c and structure. However this observation more likely reflects the limited number of samples monitored, particularly as the D_c range of undoped zirconolite-2M overlaps

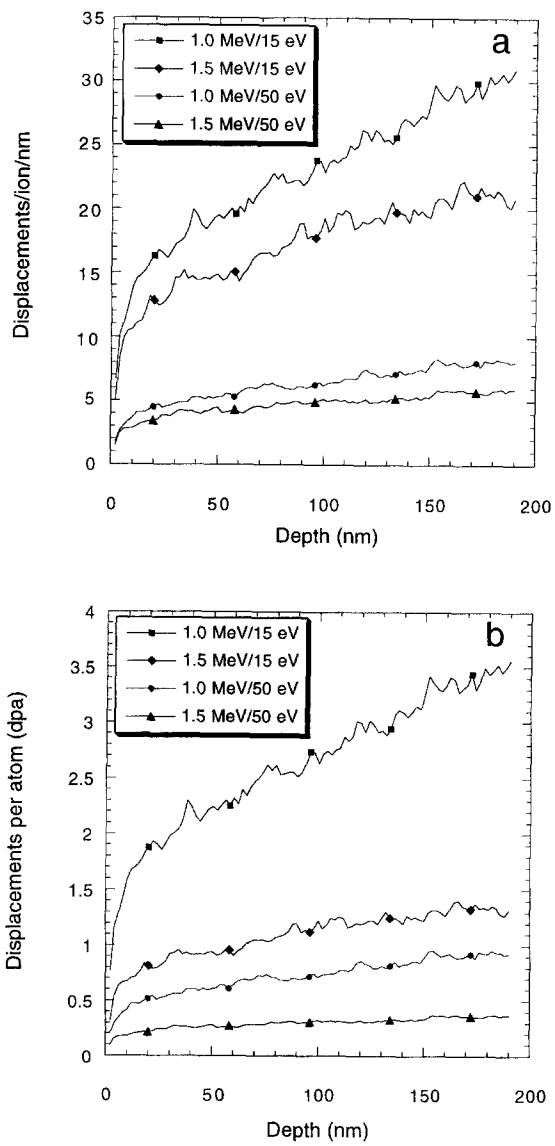

Fig. 5. (a) Displacements/ion/nm as a function of depth and (b) displacements per atom as a function of depth in zirconolite irradiated with 1.5 and 1.0 MeV Kr^+ ions. (a) was calculated using TRIM. (b) is based on TRIM calculations.

Table 2
dpa at D_c in undoped zirconolite

Ion source	Displacement energy (eV)	Range of displacements/ion/nm for zirconolite 10–190 nm thick	Critical dose for amorphisation (10^{18} ions m^{-2})	Range of dpa for undoped zirconolite 10–190 nm thick
1.0 MeV Kr^+ [a]	15	13.9–31.0	10.0 [a]	1.59–3.56
1.5 MeV Kr^+ [b]	15	10.6–20.8	5.5 [b]	0.67–1.31
1.0 MeV Kr^+ [a]	50	3.6–8.1	10.0 [a]	0.42–0.93
1.5 MeV Kr^+ [b]	50	2.8–5.9	5.5 [b]	0.18–0.37

These dpa ranges were calculated based on: TRIM derived data; D_c values measured in this and White et al.'s [11] study; and Gatehouse et al.'s [22] unit cell data for undoped zirconolite. TRIM input parameters: 2500 ions, $E_b = 2$ eV.
[a] White et al. [11].
[b] This study.

the ranges of both Nd-doped zirconolite-2M and Nd-doped zirconolite-3T. Full compositional and structural analyses of the type carried out by Hobbs et al. [32] and/or Eby et al. [30] (involving dimensionality of bonding etc.) is beyond the scope of this paper. There is no significant difference between the D_c values of crushed grains and IBT grains of Nd-doped zirconolite-4M (Table 1).

The average doses at which the zirconolite and pyrochlore superlattice maxima in SAD patterns (of zirconolite and pyrochlore respectively) first became dimmer relative to the fluorite sublattice maxima are the same ($1.4 \pm 0.5 \times 10^{18}$ ions m^{-2}) within experimental error. Diffuse rings representative of amorphous zirconolite, pyrochlore or perovksite appeared after doses of between 1.7 and 3.4×10^{18} ions m^{-2}. The Bragg diffraction maxima which persist at the highest doses in SAD patterns are those which lie on the diffuse rings representative of amorphous zirconolite, pyrochlore or perovskite. In this study, the average D_c value for the pyrochlore (4.1×10^{18} ions m^{-2}) falls within the range of the average zirconolite D_c values ($3.5–6.1 \times 10^{18}$ ions m^{-2}). The average D_c value of perovskite (18×10^{18} ions m^{-2}) is about 3–5 times larger than the average zirconolite D_c values ($3.5–6.1 \times 10^{18}$ ions m^{-2}).

The dose at which a particular SAD pattern change occurs is independent of the cross-sectional area of the monitored grain. For example, the sizes of two of the Nd-doped zirconolite-2M grains differed by a factor of 50 in area but the doses required to produce SAD pattern changes (i)–(v) were the same (within error). This is what one would expect, as the critical dimension is that closest to the beam direction (i.e., thickness), and all the grains we chose to monitor had similar thicknesses.

4.2. TRIM based calculations

The longitudinal range of 1.5 MeV Kr^+ ions in undoped zirconolite (density 4.47×10^3 kg m^{-3}) is ~490 nm (with a standard deviation ~120 nm). We estimate that the average thickness of the areas from which SAD patterns were taken was ~60 nm. Even at sample thicknesses of 200 nm, ~99% of 1.5 MeV Kr^+ ions and ~93% of 1.0 MeV Kr^+ ions are transmitted through zirconolite. Consequently, most ions would pass completely through the sample. Post-irradiation AEM analyses of irradiated samples showed no Kr.

Fig. 5a and b show displacements per ion per nanometer (displ./ion/nm) and displacements per atom (dpa) (respectively) as functions of depth (from 0 to ~200 nm) in undoped zirconolite irradiated with 1.5 and 1.0 MeV Kr^+ ions. Each of the curves represent 2500 Kr^+ ion-zirconolite interactions. At any depth, 1.0 MeV Kr^+ ions produce a greater number of dpa than 1.5 MeV Kr^+ ions.

Table 2 lists data input into TRIM, the range of disp./ion/nm values for undoped zirconolite at thicknesses of between 10 and 190 nm (calculated by TRIM), D_c values from this study and that of White et al. [11], and the corresponding calculated dpa ranges.

Variations in the thickness of the grains do not account for the factor of 2 variation in D_c (zirconolite) we have observed. The D_c required to amorphise a sample depends inversely on the average number of displ./ion/nm caused by each ion. The TRIM calculations in Fig. 5a show that when undoped zirconolite ($E_d = 15$ eV) is irradiated with 1.5 MeV Kr^+ ions, samples 30, 60 and 120 nm thick will experience approximately 11, 13 and 15 displ./ion/nm respectively. Therefore even if the thickness of the SAD monitored areas of the specimens were a factor of 2 thicker or thinner than the 60 ± 10 nm we estimate, the D_c required to render these areas amorphous would only change by ~15%.

4.3. EELS results and comments

The EELS component of this study was undertaken in order to ascertain if there were measurable differences between the EELS spectra of undamaged and damaged zirconolite. Fig. 6 shows representative examples of Ti-L_{32}

edges in EELS spectra of TiO_2, Ti_2O_3, unirradiated and irradiated undoped zirconolite. As stated previously, these spectra were collected using a SEELS system and were aligned so that the leading oxygen edges occurred at the same energy (~ 530 eV). The spectral alignment at the oxygen K edge compensated for energy drift of the spectra between successive measurements and samples. The two largest peaks in the Ti edges, L_3 and L_2, are attributable to spin orbit splitting (the excitation of electrons in the $2p_{3/2}$ and $2p_{1/2}$ subshells to unoccupied d levels). L_3 and L_2 are the lower and higher energy spin orbit peaks respectively. Molecular orbital splitting is responsible for the shoulders on the low energy sides of the L_3 and L_2 peaks (L_3^* and L_2^* respectively).

Inspection of the spectra in Fig. 6 shows that the energies of the L_3 and L_2 peaks of both unirradiated and irradiated zirconolite are similar to the energies of the L_3 and L_2 peaks of TiO_2 [33]. This suggests that Ti predominantly exhibits a valence of 4^+ in both unirradiated and irradiated zirconolite and that the bond lengths in zirconolite are similar to those in TiO_2. In addition, by comparison with reference spectra, we can determine that the change in the electron energy loss near edge structure (ELNES) of the Ti L shell is consistent with the Ti changing from octahedral coordination to tetrahedral coordination [34]. As the irradiated material is amorphous at this point, analysis of the ELNES is one of the few ways that this change in the electronic structure can be determined at the local level.

Morrison et al. [35] showed that, after background subtraction, the peaks in Fe-L_{32} edges in EELS spectra of an iron–germanium compound could be fitted with Lorentzians. Using a similar procedure, we fitted the Ti-L_{32} edges of unirradiated and irradiated undoped zirconolite with four Lorentzians in order to quantitatively measure the changes due to irradiation. From the fitted Lorentzians

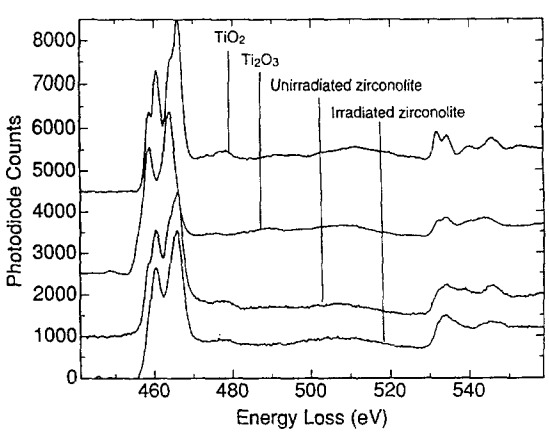

Fig. 6. EELS spectra of TiO_2, Ti_2O_3, unirradiated and irradiated zirconolite.

Table 3
EELS data

Specimen	L_2/L_3 spin orbit	L_2^*/L_3^* molecular	Energy shift L_3–L_3^* (eV)
Unirradiated undoped zirconolite	1.35	1.5	1.9
Irradiated undoped zirconolite	1.35	1.83	1.4

we calculated the ratios L_2/L_3 and L_2^*/L_3^* and the energy difference $L_3 - L_3^*$ for the spectra of unirradiated and irradiated zirconolite. Results are given in Table 3. The L_2/L_3 ratio is the same before and after irradiation which suggests that radiation damage does not significantly affect the number of holes in the d-band of the Ti (and hence the it's valence). Additional results, however, demonstrate that L_2^*/L_3^* increases and L_3–L_3^* decreases after irradiation (i.e., there is a reduction in crystal field splitting). These results suggest that radiation damage in zirconolite causes a distortion of the octahedral field around Ti atoms toward a tetrahedral configuration, consistent with previous studies of the X-ray absorption near edge structure (XANES) and the extended X-ray absorption fine structure (EXAFS) of natural zirconolite [36].

5. Discussion

5.1. Radiation damage in zirconolite, pyrochlore and perovskite

Comprehensive reviews of radiation damage effects in ceramics in general [37], and in candidate materials for high level radioactive (HLW) waste forms in particular [1], are currently available. As zirconolite, pyrochlore and perovskite are constituent phases of various HLW waste forms only a few salient facts and papers will be covered here.

(i) Ewing and Wang [12] showed that Kr^+ ion irradiation of zirconolite successfully simulates the progression of alpha decay damage in natural zirconolites. They also found that the critical dose of 1.5 MeV Kr^+ ions for amorphisation was 4×10^{18} ions m^{-2} (0.8 dpa, according to recent calculations using TRIM95 based on their original data, Wang, personal communication, 1996). Ewing and Wang's experimental and calculated results are comparable to those in this study.

(ii) Weber et al. [21] found that in natural zircon:

(a) the sequence of microstructural changes caused by heavy ion irradiation is qualitatively identical to those resulting from α-decay events;

(b) the amorphisation process is consistent with models based on the multiple overlap of particle tracks; and

(c) the amorphisation dose in displacements per atom (dpa) is nearly independent of the damage source (α-decay events or heavy ion beam irradiation) or the dose rate of heavy ions.

(iii) Lumpkin et al. [3] showed that radiation damage accumulation in natural zirconolite is consistent with models based on multiple overlap of alpha-recoil tracks and found that zirconolite became fully amorphous at a dose of 1×10^{16} α/mg (1 dpa).

There appear to be differences between the progressions of damage in different samples in this study (see for example Section 4.1.3) and between the progression of damage in zirconolite observed in this study and that observed by White et al. [11] (see Table 4). However it is our view that these apparent differences are merely due to variation in the exposure times and/or development procedures used to photograph SAD patterns.

Damage accumulation essentially occurs the same way in all zirconolite, pyrochlore and perovskite samples and is generally revealed by the following changes in the SAD patterns: weakening of superlattice maxima, appearance of diffuse rings which increase in intensity with dose, disappearance of superlattice or other specific classes of maxima, and disappearance of remaining sublattice maxima leaving only diffuse rings.

The changes in the intensity and eventual disappearance of some classes of Bragg diffraction maxima in SAD patterns of partially damaged actinide host materials suggests that some symmetry elements have been lost and that the sub-cell of the original structure has become the unit-cell of the partially damaged structure. In zirconolite and pyrochlore, the maxima which remain at high doses are representative of their fluorite sublattices. In perovskite, the maxima which remain at high doses are cubic sub-cell maxima. These observations can be accounted for if one assumes that the structure of the host is partially disrupted at the boundary between amorphous and crystalline regions.

5.2. Comparison of our results and those of White et al.

White et al. [11] made ion beam thinned TEM specimens of zirconolite samples with compositions of $CaZrTi_2O_7$, $Ca_{0.75}Gd_{0.50}Zr_{0.75}Ti_2O_7$ and $Ca_{0.75}U_{0.5}Zr_{0.75}Ti_2O_7$ and irradiated them with 1 MeV Kr^+ ions at several temperatures between 20 and 675 K using the Argonne HVEM-Tandem Facility. As in this study, White et al. monitored selected area diffraction (SAD) patterns of individual grains viewed down [110] and observed the transformation from the crystalline to amorphous state. They used the same equipment as we did, therefore the dose rates and the electron beam currents they would have used are comparable to those in this study. Consequently one would expect the room temperature D_c values of White et al. for undoped, Gd-doped and U-doped zirconolite to be similar to our results for undoped, Nd-doped and U-doped zirconolite respectively. They are not (see Table 1). Some possible reasons for discrepancies are discussed below.

5.2.1. Z dependence

White et al.'s [11] results, particularly the fact that ion beam thinning (IBT) apparently rendered their U-doped sample amorphous, led them to conclude that the radiation stability of zirconolite was strongly dependent on the incorporation of high Z dopants. We found that the radiation stability of zirconolite was independent of the atomic number of dopant species.

IBT alone is unlikely to have rendered White et al.'s sample amorphous. We found no difference in the D_c of our two zirconolite-4M samples, one of which was prepared by crushing and the other by IBT. Our U-doped zirconolite samples and those of White et al. were fabricated at 1100 and 1250°C respectively. Experiments are currently in progress to try to reproduce the U-doped zirconolite sample White et al. made, the results they got

Table 4
The transition with increasing dose of zirconolite from fully crystalline to amorphous as observed by White et al. [11] and in this study

Structural state	White et al. [11]	This study
Crystalline		
1st stage of transition	Rapid translation of strain through the sample accompanied by general diminution of intensity and increased diffuseness of Bragg reflections	The enhancement of sublattice reflections relative to other reflections.
2nd stage of transition	The disappearance of alternate (hkl), $h = k = 2n + 1$ layer lines	The appearance of diffuse rings. The disappearance of superlattice reflections. The disappearance of alternate (hkl), $h = k = 2n + 1$ layer lines
3rd stage of transition	The total removal of superlattice reflections, leaving the subcell in coexistence with an amorphous rings indicative of the onset of amorphisation	
Amorphous	Total disorder characterised by concentric amorphous rings	All Bragg reflections disappear and only diffuse rings remain

and to determine if firing temperature affects the stability of U-doped zirconolite.

5.2.2. TRIM results

Fig. 5a shows the results of theoretical calculations of displacements per ion per nanometer in undoped zirconolite as a function of depth. The pair of curves for $E_d = 15$ eV suggest that at any depth (< 190 nm), 1.0 MeV Kr^+ ions produce more damage per unit length than 1.5 MeV Kr^+ ions. Consequently, one would expect that the D_c of (~ 60 nm thick) undoped zirconolite TEM specimens irradiated with 1.0 MeV Kr^+ ions would be less than that for equivalent samples irradiated with 1.5 MeV Kr^+ ions. Contrary to this expectation, the D_c value obtained by White et al. [11] for undoped zirconolite irradiated with 1.0 MeV Kr^+ ions (at room temperature) is greater than our D_c value for undoped zirconolite irradiated with 1.5 MeV Kr^+ ions (1×10^{19} and 5.5×10^{18} Kr^+ ions m^{-2}, respectively).

Fig. 5b shows graphs of dpa versus depth in undoped zirconolite irradiated with 1.0 and 1.5 MeV Kr^+ ions. We calculated these curves on the basis of the TRIM calculations in Fig. 5a and using the D_c values measured by White et al. and in this study. Wang and Ewing [10] irradiated zircon specimens cut from the same sample with 1500 keV Xe^+, 700 and 1500 keV Kr^+ ions. They found that their samples amorphised at a constant dpa level regardless of the energy (or species) of the ion beam. Consequently one would expect the two curves in Fig. 5b generated from White et al. and our data for $E_d = 15$ eV to overlap. They do not. The following explanations could apply: (i) the dpa level required to fully amorphise zirconolite varies with energy of the irradiating ion, (ii) heavy ion irradiation effects are unreproducible, (iii) the mode (hot-pressing/sintering etc.) and/or temperature of sample fabrication affects the dpa level required to fully amorphise zirconolite or (iv) White et al. over-estimated D_c. (i) is unlikely because, as stated above, Wang and Ewing found that the dpa level required to fully amorphise zircon was independent of the energy (or species) of the ion beam. (ii) and (iii) are also unlikely as Wang and Ewing's D_c (and dpa) values for natural zirconolites are comparable to our D_c (and dpa) values for synthetic undoped zirconolites. Therefore (iv) is the most likely explanation. Our TRIM-based calculations show that if undoped zirconolite is exposed to 1×10^{19} Kr^+ ions m^{-2} (White et al.'s D_c value) and $E_d = 15$ eV, then the range of dpa values experienced by zirconolite between 10–190 nm thick is 1.7–3.6 (Table 2). All the values in this range are greater than 1.0 (the highest D_c value reported by other authors, Table 5) which suggests that White et al.'s D_c value may be high.

5.2.3. Specimen thickness

Our samples and those of White et al. [11] were 60 ± 10 nm thick and ~ 50 nm thick, respectively. Consequently, it is unlikely that the difference between our D_c values for undoped and Nd-doped zirconolite and those of White et al. for undoped and Gd-doped zirconolite can be explained by a difference in specimen thickness.

Table 5
Zirconolite D_c values measured in different studies

Material	Damage source	D_c (dpa)	Ref.
$CaZrTi_2O_7$	neutrons	~ 0.7	[8]
$CaZrTi_2O_7$	neutrons	0.4	[49]
$Ca(Zr,Cm)Ti_2O_7$	^{244}Cm	~ 0.35	[6]
$Ca(Zr,Cm)Ti_2O_7$	^{238}Pu	0.38	[5]
natural zirconolite	natural U and Th	~ 1.0	[3]
natural zirconolite	1.5 MeV Kr^+ ions	~ 0.8 [a]	[12]

[a] Recalculated using TRIM-95, see Section 5.1.

5.2.4. TEM specimen preparation

The differences between our D_c results for undoped and Nd-doped zirconolite and the D_c results of White et al. [11] for undoped and Gd-doped zirconolite are not ascribable to the fact that we prepared our TEM specimens by crushing and White et al. prepared their TEM specimens by ion beam thinning. As discussed previously, we found that the dose required to render Nd-doped zirconolite-4M amorphous was independent of whether samples were prepared by crushing or ion beam thinning.

5.3. D_c(U-doped zirconolite) versus D_c(U-doped pyrochlore)

Data from previous studies (discussed below) suggest that pyrochlore and zirconolite have approximately the same radiation resistance.

(i) AEM and microprobe studies of natural minerals show that zirconolite [3] and pyrochlore [4] require approximately the same alpha dose (1×10^{16} α/mg) to be rendered amorphous.

(ii) Karioris et al. [38] and Weber et al. [39] conducted ion irradiation studies of zirconolite, and zirconolite and pyrochlore, respectively, using the Dynamitron accelerator facility at Argonne National Laboratory, 3 MeV Ar^+ ions and XRD. Karioris et al. estimated that the damage cross-section of zirconolite for 3 MeV Ar^+ ions was 0.07 nm^2; whereas Weber et al. estimated that the damage cross-section of zirconolite and pyrochlore for 3 MeV Ar^+ ions were 0.014 and 0.023 nm^2, respectively. The reason for the discrepancy between zirconolite results is not understood. In conjuction, the results of Karioris et al. and Weber et al. suggest that the radiation resistance of pyrochlore and zirconolite vary by a factor of between 2 and 3. For comparison, the spread of D_c values of all the zirconolites in this study (apart from outliers) can be accommodated by a factor of 2.

(iii) The investigation by Weber et al. [6] of self-radiation damage in synthetic Cm-doped $Gd_2Ti_2O_7$ (pyrochlore) and $CaZrTi_2O_7$ (zirconolite) showed that pyrochlore and zirconolite became amorphous at alpha doses of 3.8 and 5×10^{15} α/mg respectively (i.e., they vary by a factor less than that describing the full range of values for our zirconolites).

As one might expect from the similarity of the structures of zirconolite and pyrochlore, and in general agreement with the results of previous authors, we found that the D_c values of U-doped zirconolite and pyrochlore irradiated with 1.5 MeV Kr^+ ions are comparable ($\approx 4 \times 10^{18}$ ions m^{-2}). The fact that our result (D_c(pyrochlore) ≈ D_c(zirconolite)) mimics what is found in natural samples, lends weight to the use of heavy ion irradiation as a method for determining the relative alpha-decay radiation resistance of different phases.

5.4. D_c(perovskite) versus D_c(zirconolite)

Data from natural samples as to the relative radiation resistance of perovskite and zirconolite is not conclusive. D_c(zirconolite) is well constrained and lies somewhere between 0.8 and 1.2×10^{16} α/mg [3]. D_c(perovskite) is less certain. Data on several natural perovskites collated by Van Konynenburg and Guinan [40] indicates that D_c(perovskite) lies between 0.3 and 2.6×10^{16} α/mg. Sinclair and Ringwood [25] reported a personal communication from 'Kogarko', who stated that loparites (rare-earth-rich perovskites) found in the Lovozero intrusion, Kola Peninsula in the former USSR, still produced sharp X-ray diffraction (XRD) patterns after they had accumulated a dosage of 0.89×10^{16} α/mg. However we have analysed 3 samples from that location and (based on their composition and age) we estimate that they have only experienced between 0.02 and 0.5×10^{16} α/mg. So in summary, data from natural samples suggest that D_c(perovskite) lies somewhere between ~ 0.5 and 2 times D_c(zirconolite).

As discussed earlier (Section 5.3), Karioris et al. [38] and Weber et al. [39] reported that the damage cross-section of zirconolite exposed to 3 MeV Ar^+ ions was 0.07 and 0.014 nm^2, respectively. Karioris et al. also reported that the damage cross-section of perovskite exposed to 3 MeV Ar^+ ions was 0.32 nm^2. On this basis, one would expect perovskite to amorphise more readily than zirconolite.

In Section 5.2, we have disputed White et al.'s [11] room temperature D_c values for zirconolite. However we have no basis for dispute of their data collected at 20 K, which suggests that zirconolite ($Ca_{0.75}Gd_{0.50}Zr_{0.75}Ti_2O_7$) amorphises (three times) more readily than perovskite ($Ca_{0.8}Gd_{0.2}TiO_3$) when exposed to 1.0 MeV Kr^+ ions. They did not report room temperature results for perovskite.

Hough and Marples [41] found that at a dose of 8×10^{15} α/mg, the dose-dependent macroscopic swelling of single phase Pu-doped zirconolite (and polyphase Synroc containing zirconolite and perovskite) had saturated while that of single phase Pu-doped perovskite was still increasing. This suggests that perovskite is more radiation resistant than zirconolite. However, the relationship between macroscopic swelling and amorphisation is not simple. For example, Mosley [42] showed that perovskite-structured $CmAlO_3$ continued to swell after it became amorphous.

Table 6
Comparison of the structures of zirconolite, pyrochlore and perovskite ($CaTiO_3$) and their parent structures (fluorite, fluorite and cubic perovskite respectively)

	Type of bonding	Type of packing	Number of cations in a formula unit (and their coordination numbers)	Number of anions in a formula unit	Number of atoms in the unit cell	Unit cell volume (Å^3)
Fluorite	ionic	SCP [a]	1 (8)	1	12	~ 130 [c]
Pyrochlore	mixed	distorted SCP [a]	2 (8,6)	2	88	~ 1030 [d]
Zirconolite	mixed	distorted SCP [a]	5 (8,7,6,5)	7	88	~ 1040 [e]
Cubic perovskite	ionic	Ca and O are in CCP [b]	1 (12,6)	1	5	~ 60 [f]
Orthorhombic perovskite ($CaTiO_3$)	ionic	Ca and O are in slightly distorted CCP [b]	4 (12,6)	4	20	224 [g]

[a] Simple cubic packing.
[b] Cubic close packing.
[c] Bloss [18].
[d] Chakoumakos [50].
[e] Gatehouse et al. [22].
[f] Reller [51].
[g] Koopmans et al. [52].

Consequently, without microstructural examination, it would be premature to interpret Hough and Marples' macroscopic swelling results in terms of which phase (zirconolite or perovskite) is more radiation resistant.

Mosley [42] also found that $CmAlO_3$ became X-ray amorphous a dose of ~ 0.2 dpa (0.3×10^{16} α/mg). This is comparable to the doses at which ^{238}Pu and ^{244}Cm doped zirconolite become X-ray amorphous (0.3×10^{16} α/mg [43] and 0.5×10^{16} α/mg [6] respectively).

We found that the dose required to render perovskite amorphous (18×10^{18} ions m^{-2}) is (3–5 times) greater than the dose required amorphise zirconolite ($3.5–6.1 \times 10^{18}$ ions m^{-2}). Our results agree with the relative radiation resistance of zirconolite and perovskite found by White et al. [11] (who irradiated zirconolite and perovskite with 1.0 MeV Kr^+ ions at 20 K). However they disagree with (i) the relative radiation resistance of zirconolite and perovskite reported by Karioris et al. [38] (who irradiated zirconolite and perovskite with 3.0 MeV Ar^+ ions at room temperature) and (ii) what one would expect from studies of perovskite-structured $CmAlO_3$ and actinide-doped zirconolite and perovskite [42,6,43].

5.5. The relative radiation resistance of zirconolite, pyrochlore and perovskite

Our observations that D_c(zirconolite) $\approx$ D_c(pyrochlore) $<$ D_c(perovskite) are in line with what one would expect given the structures of these phases. As discussed by Naguib and Kelly [44], Eby et al. [30] and Wang et al. [31], the radiation damage susceptibility of a compound depends on:

(i) the nature of its bonding (compounds exhibiting covalent bonding damage more readily than those exhibiting mixed or ionic bonding);

(ii) whether the material exhibits open or close-packing (e.g., compounds exhibiting simple cubic packing are more susceptible to damage than those exhibiting cubic close packing) and

(iii) its topologic and chemical complexity (damage susceptibility increases with the number of cation and anion sites and their corresponding coordination numbers, the total number of atoms in the unit cell and the unit cell volume).

Table 6 shows that zirconolite and pyrochlore have comparable structures in terms of bonding packing, topologic and chemical complexity and that perovskite is topologically simpler than these phases. Given these data, it is not surprising that we found that D_c(zirconolite) $\approx$ D_c(pyrochlore) $<$ D_c(perovskite).

5.6. More comments on and implications of the TRIM calculations

Our results (Fig. 5b) suggest that when undoped zirconolite is irradiated to D_c with 1.5 MeV Kr^+ ions, material at a depth of 100 nm will have experienced ~ 1.2 dpa. Ewing and Wang's [12] data for undoped zirconolite irradiated with 1.5 MeV Kr^+ ions, recalculated by Wang (personal communication, 1996, Table 5), suggests that material at a depth of 100 nm will have experienced ~ 0.8 dpa. The difference between these results is accounted for by the fact that we estimate D_c(undoped zirconolite) to be 5.5×10^{18} ions m^{-2} and Ewing and Wang estimated it to be 4.0×10^{18} ions m^{-2}.

D_c(zirconolite) values determined by previous authors (Table 5) vary from ~ 0.35 to ~ 1.0 dpa (i.e., by a factor of ≈ 3). Our D_c(zirconolite) values vary by a similar factor (≈ 2).

Data reported by previous authors (Table 5) and our TRIM data suggest that an E_d value of 15 eV (as used by Ewing, Wang and co-workers, e.g., Ewing and Wang [12]) is appropriate for zirconolite. From Table 5, one can assume that when zirconolite is subjected to D_c the majority of the specimen will have experienced at least 0.35 dpa. TRIM-based calculations (Fig. 5) show that if E_d of undoped zirconolite is 50 eV, then when undoped zirconolite is exposed to 5.5×10^{18} 1.5 MeV Kr^+ ions m^{-2} (our D_c value), only zirconolite at depths of > 150 nm will experience ≥ 0.35 dpa (i.e., be amorphous). However we estimate that our samples are only ~ 60 nm thick. Similar TRIM-based calculations show that if $E_d = 15$ eV, then all undoped zirconolite thicker than 2 nm will experience ≥ 0.3 dpa. This supports Ewing and Wang's use of $E_d = 15$ eV.

5.7. Discussion of EELS results

After irradiation, we found that the Ti L_2/L_3 ratio remained unchanged, the Ti L_2^*/L_3^* ratio increased, and the Ti L_3–L_3^* value decreased (Table 3). The former result suggests that radiation damage does not significantly affect the valence of Ti. The two latter results indicate a reduction in crystal field splitting which suggests that radiation damage in zirconolite causes a distortion of the octahedral field around Ti atoms. Analysis of the ELNES of the Ti L shell using reference spectra further indicates that the distortion involves a change from an octahedral toward a tetrahedral configuration of oxygen atoms around Ti.

Previously, Lumpkin et al. [36] and Farges et al. [45] used XANES and EXAFS to investigate natural amorphous and annealed zirconolite samples. Lumpkin et al. suggested that radiation damage of zirconolite results in increased distortion of the octahedral field around Ti atoms, a decrease in the coordination number of Ti and Ca, and a reduction in Ti–O bond lengths. Farges et al. found no significant change in the local environment of Zr and Th and suggested that primary effect of radiation damage is polyhedral tilting, resulting in the loss of long-range periodicity and a reduction of medium-range order. Although some polyhedral tilting must be invoked (i.e., increased M–O–M angles and M–M distances) in order to explain

the volume expansion observed by Lumpkin et al., our results obtained using EELS also indicate that radiation damage causes a measurable distortion of the local environment around the Ti atoms in zirconolite.

In EELS, the extended electron energy loss fine structure (EXELFS) and ELNES are directly analogous to EXAFS and XANES so, in theory, the information obtained from these techniques can be used to give accurate bond lengths and coordination numbers. However, the information available from EELS is limited by (i) the lower intensity energy source of the gun in an electron microscope, (ii) difficulties associated with background subtraction, and (iii) the limited energy range available for data collection at low energies (e.g., [46,47]). Furthermore, the use of SEELS requires long collection times and may involve the additional effects of contamination and electron beam damage. Recently developed parallel detection (PEELS) systems have overcome some of these problems, allowing high-resolution spectra to be acquired in a relatively short period of time. PEELS data are well suited to the analysis of ELNES at a level comparable to that of XANES as demonstrated in several recent investigations (e.g., [47,48]). Unlike EXAFS, EXELFS is unlikely to be broadly applicable to materials due to the relatively weak modulations and poor energy resolution. For example, typical edge spacings of 100–200 eV in EELS spectra limit the accuracy of bond length information derived from EXELFS to 0.02–0.03 nm, approximately an order of magnitude larger than the accuracy obtainable from EXAFS data [45–47]. However EXELFS may be useful in applications where only limited sample is available, as the minimum sample volume required for EXELFS ($\sim 10^{-23}$ m^3) is much smaller than that required for EXAFS ($\sim 10^{-7}$ m^3).

6. Conclusions

Using 1.5 MeV Kr^+ ions, we observed that damage accumulation essentially occurs in the same way in zirconolite, pyrochlore and perovskite. The progression of damage is generally revealed by the following changes in SAD patterns: weakening of superlattice maxima, appearance of diffuse rings which increase in intensity with dose, disappearance of superlattice or other specific classes of maxima, and disappearance of remaining sublattice maxima leaving only diffuse rings.

The average critical doses for amorphisation (D_c) at which all the zirconolites (undoped, Nd-doped, U-doped and Th-doped) and the pyrochlore in this study became fully amorphous varied by a factor of ~ 2 (from 3.6 to 6.1×10^{18} ion m^{-2}).

The data collected in this study show that there are no correlations between the critical dose for amorphisation, D_c, and the atomic weight of dopants in zirconolite or between D_c and the mean atomic weight of the sample.

As one would expect from the similarity of their structures, the D_c values of U-doped pyrochlore is comparable to that of U-doped zirconolite (as is observed in natural samples and Cm-doped synthetic samples). This result confirms that heavy ion irradiation is a good mimic of alpha-decay damage.

The D_c value at room temperature of perovskite irradiated with 1.5 MeV Kr^+ ions is 1.8×10^{19} ions m^{-2}. This is about 3–5 times the zirconolite D_c value. This latter observation is in line with what one would expect from the relative topologic and chemical complexity of the two phases.

This study shows that EELS can be used to monitor radiation-induced structural changes in zirconolite and that EELS indicates the same sort of changes seen by previous authors using XANES and EXAFS.

Acknowledgements

The authors thank the HVEM-Tandem Facility staff at Argonne National Laboratory for assistance during ion irradiations. The Facility is supported as a User Facility by the US DOE, Basic Energy Sciences, under contract W-31-109-ENG-38. The authors thank Peter Fielding of the University of New England, NSW, Australia, Lou Vance of ANSTO and Alan Coelho of the University of Technology, Sydney, Australia, for making and kindly providing, the undoped and Th-doped zirconolite, the U-doped zirconolite and pyrochlore, and the Nd-doped zirconolites respectively. The perovskite sample was kindly provided by Bob Middleton of the Academy of Sciences, Philadelphia, PA, USA. K.L.S. thanks Lou Vance for comprehensive editing and Mike Colella for technical assistance with this manuscript.

References

[1] R.C. Ewing, W.J. Weber, F.W. Clinard Jr., Prog. Nucl. Energy 29 (2) (1995) 63.
[2] K.L. Smith, G.R. Lumpkin, M.G. Blackford, R.A. Day, K.P. Hart, J. Nucl. Mater. 190 (1992) 287.
[3] G.R. Lumpkin, R. Giere, K.P. Hart, P.J. McGlinn, T.E. Payne, Radiochim. Acta 66&67 (1994) 469.
[4] G.R. Lumpkin, R.C. Ewing, Phys. Chem. Miner. 16 (1988) 2.
[5] F.W. Clinard, Ceram. Bull. 65 (1986) 1181.
[6] W.J. Weber, J.W. Wald, Hj. Matzke, J. Nucl. Mater. 138 (1986) 196.
[7] H. Mitamura, S. Matsumoto, K.P. Hart, T. Miyazaki, E.R. Vance, Y. Tamura, Y. Togashi, T.J. White, J. Am. Ceram. Soc. 75 (1992) 392.
[8] K.D. Reeve, J. Woolfrey, J. Aust. Ceram. Soc. 16 (1980) 10.
[9] Hj. Matzke, J.L. Whitton, Can. J. Phys. 44 (1966) 995.
[10] L.M. Wang, R.C. Ewing, Nucl. Instrum. Meth. B65 (1992) 324.

[11] T.J. White, R.C. Ewing, L.M. Wang, J.S. Forrester, C. Montross, Mater. Res. Soc. Symp. Proc. 353 (1995) 1413.
[12] R.C. Ewing, L.M. Wang, Nucl. Instrum. Meth. B65 (1992) 319.
[13] J. Ziegler, J.P. Biersack, U. Littmark, The Stopping Range of Ions in Solids (Pergamon Press, New York, 1985).
[14] K.L. Smith, G.R. Lumpkin, Defects and Processes in the Solid State: Geoscience Applications, The McLaren Volume, Elsevier Monograph Series (Elsevier, Amsterdam, 1993) p. 401.
[15] P. Bayliss, F. Mazzi, R. Munno, T.J. White, Mineral. Mag. 53 (1989) 565.
[16] P.E. Fielding, T.J. White, J. Mater. Res. 2 (1988) 387.
[17] F.W. Clinard, L.W. Hobbs, C.C. Land, D.E. Peterson, D.L. Rohr, R.B. Roof, J. Nucl. Mater. 105 (1982) 248.
[18] F.D. Bloss, Crystallography and Crystal Chemistry (Mineralogical Society of America, 1994).
[19] E.R. Vance, C.J. Ball, M.G. Blackford, C.J. Cassidy, K.L. Smith, J. Nucl. Mater. 175 (1990) 58.
[20] M.G. Blackford, J. Electron. Mic. Techn. (1996) submitted.
[21] W.J. Weber, R.C. Ewing, L.M. Wang, J. Mater. Res. 9 (1994) 688.
[22] B.M. Gatehouse, I.E. Grey, R.J. Hill, H.J. Rossell, Acta Crystallogr. B37 (1981) 306.
[23] G.P. Pells, J. Nucl. Mater. 155–157 (1988) 67.
[24] R.C. Ewing, T.J. Headley, J. Nucl. Mater. 119 (1983) 102.
[25] W. Sinclair, A.E. Ringwood, Geochem. J. 15 (1981) 229.
[26] M.C. Wittels, F.A. Sherrill, J. Appl. Phys. 28 (1957) 606.
[27] J. Koike, P.R. Okamoto, L.E. Rehn, M. Meshii, Mater. Res. Symp. (1989).
[28] M.T. Robinson, J. Nucl. Mater. 216 (1994) 1.
[29] P.S. Turner, T.J. White, A.J. O'Connor, C.J. Rossouw, J. Microsc. 162 (1991) 369.
[30] R.K. Eby, R.C. Ewing, R.C. Birtcher, J. Mater. Res. 7 (11) (1992) 3080.
[31] L.M. Wang, R.K. Eby, J. Janeczek, R.C. Ewing, Nucl. Instrum. Meth. B59&60 (1991) 395.
[32] L.W. Hobbs, A.N. Sreeram, C.E. Jesurum, B.A. Berger, Nucl. Instrum. Meth. B116 (1996) 18.
[33] R. Brydson, B.G. Williams, W. Engel, H. Sauer, E. Zeitler, J.M. Thomas, Solid State Commun. 64 (1987) 609.
[34] R. Brydson, L.A.J. Garvie, A.J. Craven, H. Sauer, F. Hofer, G. Cressey, J. Phys.: Condens. Matter 5 (1993) 9379.
[35] T.I. Morrison, M.B. Brodsky, N.J. Zaluzec, Phys. Rev. B35 (5) (1985) 3107.
[36] G.R. Lumpkin, R.C. Ewing, B.C. Chakoumakos, R.B. Greegor, F.W. Lytle, E.M. Foltyn, F.W. Clinard Jr., L.A. Boatner, M.M. Abraham, J. Mater. Res. 1 (1986) 564.
[37] L.W. Hobbs, F.W. Clinard Jr., S.J. Zinkle, R.C. Ewing, J. Nucl. Mater. 216 (1994) 291.
[38] F.G. Karioris, K. Appaji Gowda, L. Cartz, J.C. Labbe, J. Nucl. Mater. 108&109 (1982) 748.
[39] W.J. Weber, N.J. Hess, G.D. Maupin, Nucl. Instrum. Meth. B65 (1992) 102.
[40] R.A. Van Konynenburg, M.W. Guinan, Nucl. Technol. 60 (1983) 206.
[41] A. Hough, J.A.C. Marples, The radiation stability of Synroc: Final report AEA Technology Report, AEA-FS ~ 0201(H), 1993.
[42] W.C. Mosley, J. Am. Ceram. Soc. 54 (1971) 475.
[43] F.W. Clinard, D.L. Rohr, R.B. Roof, Nucl. Instrum. Meth. B1 (1984) 581.
[44] H.M. Naguib, R. Kelly, Radiat. Eff. 25 (1975) 1.
[45] F. Farges, R.C. Ewing, G.E. Brown Jr., J. Mater. Res. 8 (1993) 1983.
[46] D.C. Joy, A.D. Romig Jr., J.I. Goldstein, Principles of Analytical Electron Microscopy (Plenum, New York, 1986).
[47] L.A.J. Garvie, A.J. Craven, R. Brydson, Am. Mineral. 79 (1994) 411.
[48] L.A.J. Garvie, A.J. Craven, Phys. Chem. Miner. 21 (1994) 191.
[49] G.R. Lumpkin, K.L. Smith, R.G. Blake, Mater. Res. Soc. Symp. Proc. 412 (1996) 329.
[50] B.C. Chakoumakos, J. Solid State Chem. 53 (1984) 120.
[51] A. Reller, Philos. Mag. A68 (1993) 641.
[52] H.J.A. Koopmans, G.M.H. Van de Velde, P.J. Gellings, Acta Crystallogr. C39 (1983) 1323.